

Electron Spin Coherences in Rare-Earth Optically Excited States for Microwave to Optical Quantum Transducers

Sacha Welinski,¹ Philip J. T. Woodburn,² Nikolai Lauk,³ Rufus L. Cone,² Christoph Simon,³ Philippe Goldner,¹ and Charles W. Thiel²

¹*PSL Research University, Chimie ParisTech, CNRS,
Institut de Recherche de Chimie Paris, 75005, Paris, France*

²*Department of Physics, Montana State University, Bozeman, MT 59717, USA*

³*Institute for Quantum Science and Technology and Department of Physics and Astronomy,
University of Calgary, Calgary AB T2N 1N4, Canada*
(Dated: October 24, 2018)

Efficient and reversible optical to microwave coherent transducers are required to enable entanglement transfer between superconducting qubits and light for quantum networks. Rare-earth-doped crystals that possess narrow optical and spin transitions are a promising way to implement these devices. Current approaches use ground-state electron spin transitions that have coherence lifetimes (T_2) often limited by spin flip-flop processes and/or spectral diffusion, even at very low temperatures. Here, we investigate spin coherence in an optically excited state of an $\text{Er}^{3+}:\text{Y}_2\text{SiO}_5$ crystal at temperatures from 1.6 to 3.5 K and under a weak 8.7 mT magnetic field. Spin coherence and population lifetimes of up to 1.6 μs and 1.2 ms, respectively, are measured by 2- and 3-pulse optically-detected spin echo experiments. Analysis of the dephasing processes suggest that ms T_2 can be reached at lower temperatures for the excited-state spins, whereas ground-state spin states could be limited to a few μs due to resonant interactions with the other Er^{3+} spins in the lattice (spin diffusion). We propose a quantum transducer scheme with the potential for close to unit efficiency that exploits the specific advantages offered by the spin states of optically excited electronic energy levels.

Rare-earth (RE) doped crystals can exhibit long optical and spin coherence lifetimes at liquid helium temperatures that are promising for optical quantum technologies [1–3]. For example, long lived quantum memories for light [4], entanglement storage [5], light to matter teleportation [6], as well as atomic gas to crystal quantum state transfer [7] have all been demonstrated in bulk materials. Developments towards integrated and hybrid systems have also been reported using nano-structured materials [8, 9], making RE doped crystals a promising platform for solid-state quantum light-to-matter interfaces. In this respect, RE ions with an odd number of electrons are of particular interest since their strong magnetism offers the capability to efficiently couple to microwave photons. This could enable quantum-state transfer between superconducting qubits and light to build networks of quantum processors, for example [10, 11]. Strong coupling between superconducting resonators and RE ions has been achieved, and microwave to optical conversion efficiencies have been investigated [12–15].

Using both optical and spin transitions requires strong coupling between light and microwaves. Ensembles of RE ions in crystals are generally employed in applications to enhance the interaction efficiency with light. While providing a number of advantages, ensembles also lead to specific difficulties when considering potential optical to spin coherence transfer processes. In particular, the weak optical oscillator strengths limit addressable bandwidths for π pulses typically to much less than 100 MHz; however, optical inhomogeneous linewidths are usually of the order of 1 GHz or larger [1], which means that a

majority of ions, and therefore spins, do not participate in the coherent excitation process and are only ‘spectators’. When a coherence is stored in a superposition of the ground-state electron spin states, two undesirable issues may appear. First, the excitation can be incoherently transferred by fast spin flip-flops, or spin diffusion, to other spins in the lattice, including the large number of spectator spins, resulting in decoherence and loss of the stored quantum state. Secondly, to efficiently drive the spin transition, pulses with bandwidths as large as the spin inhomogeneous linewidths are required since there is generally no correlation between optical and spin frequencies within the respective inhomogeneous linewidths. However, these high-bandwidth control pulses will also drive a large number of spectator spins, potentially causing significant decoherence by instantaneous spectral diffusion (ISD) due to long-range spin-spin interactions [14]. Paramagnetic RE ions can exhibit significant spin-spin interactions even for RE concentrations as low as 10 ppm [16]. As a result, these interactions often cannot be eliminated by reducing the ion concentration without also reducing the optical absorption and limiting the ultimate device efficiency.

We propose to circumvent these limitations by using spin transitions for optically excited electronic states. In this case, the optically excited ions are no longer resonant with the much larger number of spectator spins in the lattice, minimizing decoherence due to the flip-flop process. Furthermore, only optically excited spins are resonant with the microwave fields, avoiding excitation of spectator spins by the control pulses and reducing ISD

to the lowest possible extent. While this scheme is fundamentally limited by the excited-state population lifetime $T_{1,\text{opt}}$, this can be longer than ms for RE ions, meeting the requirements for microwave-optical transduction protocols. A particularly favorable ion is erbium with typical excited-state lifetimes of ~ 10 ms for the $^4I_{13/2}$ level [17]. This $1.5\ \mu\text{m}$ telecom wavelength transition has also attracted strong interest for building fiber-based quantum networks and transducers [13, 15, 18].

Here, we investigate electron spin coherence in the excited state of an Er^{3+} doped Y_2SiO_5 crystal, and observe, for the first time to our knowledge, excited-state electron spin echoes for RE ions. Coherence lifetimes of up to $1.6\ \mu\text{s}$ at 1.9 K and with a field of 8.7 mT were measured using coherent optical detection. Analysis of the decoherence mechanisms suggests that T_2 of up to several ms can be obtained at lower temperatures, whereas ground-state spin coherences are limited to much shorter lifetimes due to flip-flop processes. Excited-state spin transitions can therefore be an attractive option for microwave to optical transduction at telecom wavelengths and we present and analyze an excited-state transduction protocol that can reach close to unity efficiency.

Experiments were performed using coherent Raman heterodyne scattering (RHS) techniques [19] for the three-level schemes shown in Fig. 1. This method employs a radio-frequency (RF) field resonant with a Zeeman transition $|1\rangle \leftrightarrow |2\rangle$ or $|3\rangle \leftrightarrow |4\rangle$ to create a ground- or excited-state electron spin coherence (Fig. 1A). A resonant, or near resonant, laser beam drives the optical transition $|1\rangle \leftrightarrow |3\rangle$ or $|1\rangle \leftrightarrow |4\rangle$. The combined optical and RF coherences then induce a coherence on the other optical transition $|2\rangle \leftrightarrow |3\rangle$ or $|1\rangle \leftrightarrow |3\rangle$ that then interferes with the laser field, producing a beat note at the $|1\rangle \leftrightarrow |2\rangle$ or $|3\rangle \leftrightarrow |4\rangle$ frequencies that can be detected using a fast photodiode placed after the sample.

We use a 50 ppm Er^{3+} -doped YSO sample grown by Scientific Materials Inc. (Bozeman, MT) and cut along the three dielectric axes: b , D_1 , D_2 [20]. Er^{3+} can substitute for Y^{3+} at two inequivalent crystallographic sites (denoted 1 and 2). Furthermore, each site has two subgroups with different local site orientations and exhibit different Zeeman effects unless the magnetic field is applied either parallel or perpendicular to the b axis. The sample was mounted in an Oxford Optistat helium cryostat with a magnetic field generated by a Helmholtz coil applied along D_1 . A New Focus Velocity diode laser was set at 1536.49 nm (vacuum) in resonance with the transition between the lowest crystal field levels of the $^4I_{15/2}$ and $^4I_{13/2}$ multiplets for ions at site 1. The optical inhomogeneous linewidth was 390 MHz for the sample studied. The laser propagated along the crystal's b axis and was polarized along the D_1 axis. The CW laser incident on the crystal produced nearly equal populations in both the ground and excited states over approximately 1 MHz bandwidth. Optical pumping also induced popula-

tion differences within the ground- and excited-state Zeeman sub-levels necessary to detect spin coherence with the RHS method. Transmitted light was detected by a New Focus model 1611 photoreceiver with a 1 GHz bandwidth. RF pulses with magnetic field along b were applied to the sample through a copper wire RF waveguide held next to the crystal surface.

Fig. 1B shows the RHS spectra for frequencies of up to 1 GHz as a function of magnetic field strength. In these experiments, an RF spectrum analyzer was used to generate the constant RF excitation signal and to also analyze the photoreceiver signal. The four straight lines observed in Fig. 1B correspond to electron-spin transitions for the ground and excited states of Er^{3+} isotopes with zero nuclear spin, as deduced from the magnetic field direction and known \mathbf{g} tensors [21, 22]. Two transitions are observed for each state since the magnetic field was not exactly parallel to D_1 , resulting in two inequivalent sub-groups for each site. The corresponding effective ground-state values g_g are 4.75 and 3.85 (± 0.3), and the excited-state values g_e are 4.35 and 3.27 (± 0.3), depicted in Fig. 1C). These measured values allow us to determine the exact direction of the magnetic field with respect to the bD_1D_2 crystal frame: $\theta = 86.91 \pm 0.01^\circ$ and $\phi = 7.0 \pm 0.2^\circ$. All of the spin transitions exhibited linewidths of approximately 10 MHz, similar to those previously reported [15, 21]. No significant variation in linewidth with magnetic field strength was observed, indicating that the broadening of the spin transitions do not arise from inhomogeneity in the \mathbf{g} tensors. Other transitions with more complex field dependence are also visible in Fig. 1B) and are attributed to hyperfine transitions of the $^{167}\text{Er}^{3+}$ isotope ($I = 7/2$, abundance 22.9 %).

Excited-state spin echoes were measured using RF pulses generated by a gated source. The signal from the photoreceiver was amplified, filtered, and then down mixed with a local oscillator signal (see Supplemental Material). The magnetic field was fixed at 8.7 mT with the same orientation as for the CW experiments, and the RF frequency was set at 400 MHz to study the excited-state transition (Fig. 1C). Experiments were performed as a function of temperature in the range from 1.6 to 3.5 K, with the sample in superfluid LHe below 2.1 K and in a constant flow of He exchange gas for higher temperatures.

The signal for the 2-pulse echo sequence is shown in Fig. 2A for two different delays between the excitation and rephasing pulses. Pulse lengths of 150 ns were optimized for maximum echo amplitude. The echo amplitude has an opposite sign as the excitation and rephasing pulses, confirming that the entire sequence was phase coherent. The large excited-state population created by the CW laser excitation allowed strong echo signals to be produced. By varying the delay between the first and the second pulse, we measured the decay of the integrated

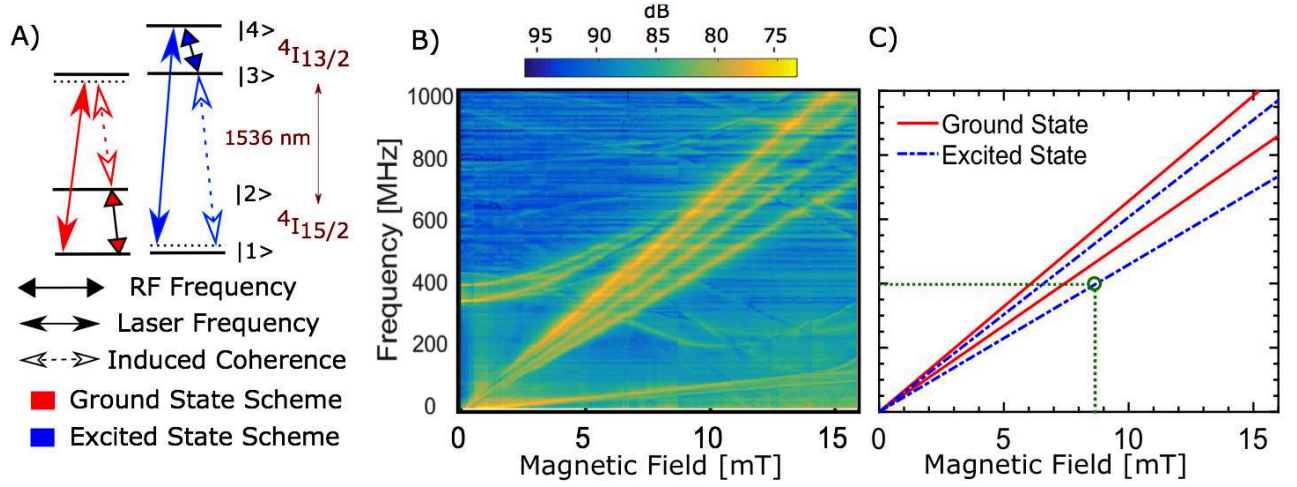


FIG. 1. A) Energy level structure of Er^{3+} and RHS schemes for ground- and excited-state spin coherence studies ($|1\rangle \leftrightarrow |2\rangle$ and $|3\rangle \leftrightarrow |4\rangle$ are electron spin transitions). B) RHS measurements at 3 K on Er^{3+} at site 1 of Y_2SiO_5 with the magnetic field aligned close to the D_1 axis. C) Fitted Zeeman transition frequencies for the zero-nuclear-spin Er^{3+} isotopes. The green circle indicates the conditions used for spin echo measurements.

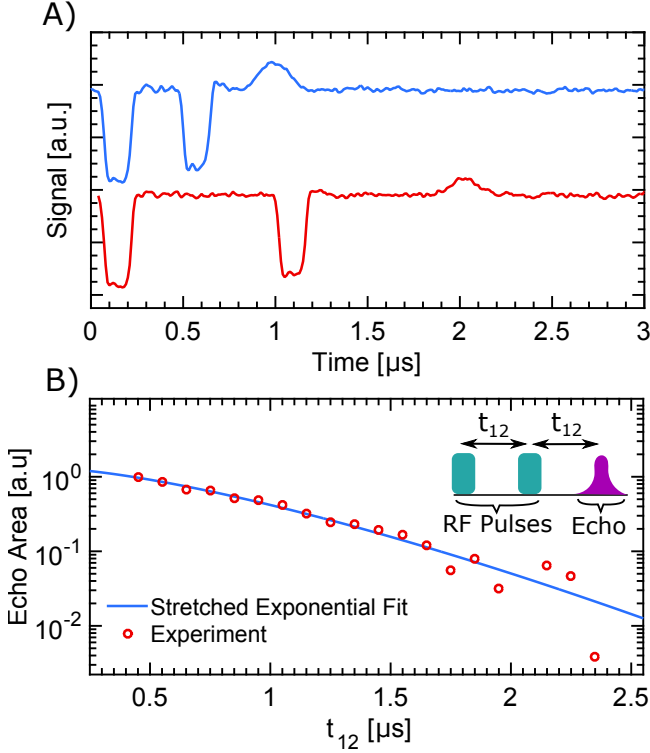


FIG. 2. A) Examples of optically detected electron spin echoes in the $^4\text{I}_{13/2}$ excited state for different pulse delays with $T = 1.9$ K and $B = 8.7$ mT. B) Measurement (circles) and fit (line) of echo area decay at 1.9 K, giving $T_2 = 1.6 \pm 0.2$ μs and $x = 1.4 \pm 0.2$. Inset: RF pulse sequence.

area of the echo signal (Fig. 2B). It was fitted with a Mims decay shape [23]: $A(\tau) = A \exp[-(2t_{12}/T_{2e})^x]$ where T_{2e} is the $1/e$ phase coherence lifetime and t_{12} is

the time delay between excitation and rephasing pulses. The extracted T_{2e} at 1.9 K was 1.6 ± 0.2 μs (200 kHz homogeneous linewidth), with $x = 1.4 \pm 0.2$. The non-exponential behavior indicates a spectral diffusion effect due to interactions with the bath of Er^{3+} spins in the lattice [23]. The effect of ^{89}Y nuclear spins is expected to be much smaller because of their weak magnetic moment and slow flip rates [24]. Due to the narrow bandwidth of the optical excitation, the excited-state ion concentration for site 1 is $\sim 10^3$ times lower than ground-state concentration and do not contribute significantly to spectral diffusion. At the Er^{3+} concentration and low magnetic fields studied here, ground-state spins are only weakly polarized for both sites and are expected to relax mainly by mutual spin flip-flop processes (spin diffusion) even at very low temperatures.

To probe the source of decoherence, we performed 3-pulse stimulated spin echo measurements. The pulse sequence is shown in Fig. 3A. The stimulated echo decays during the delay t_{23} between the second and third pulse from both spin relaxation and spectral diffusion, allowing the dynamics to be studied over the longer T_1 time scale, whereas 2-pulse echoes are limited to the T_2 time scale [23, 24]. We measured 3-pulse echo decays as a function of t_{23} , with t_{12} fixed at 0.3 μs at temperatures between 1.6 and 3 K. An example is shown in Fig. 3A. An initial fast decay due to spectral diffusion is observed on short time scales, whereas the slower exponential decay at longer delays corresponds to population relaxation.

Spectral diffusion in 2 and 3 pulse echoes can be modeled by a time-dependent effective homogeneous linewidth Γ_{eff} [24], where the echo amplitude is given

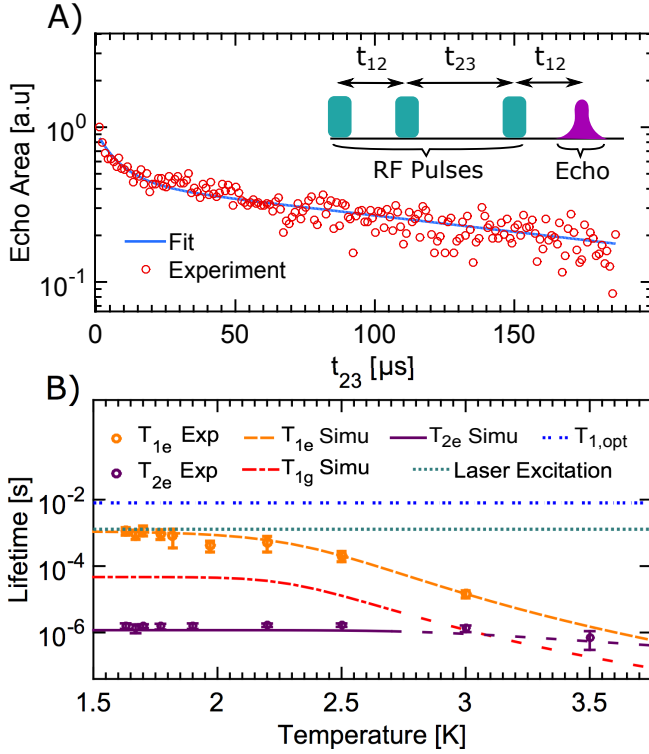


FIG. 3. A) Excited-state electron spin stimulated echo decay measured at 2.5 K (circles) and fit to the spectral diffusion model (line, see text). Inset: RF pulse sequence. B) Experimental and modeled coherence and population lifetimes as a function of temperature.

by:

$$A(t_{12}, t_{23}) = A_0 e^{(-\frac{t_{23}}{T_{1e}})} e^{[-2t_{12}\pi\Gamma_{eff}(t_{12}, t_{23})]}. \quad (1)$$

The excited-state spins probed in the echo sequence interact with the bath of ground-state site 1 Er^{3+} spins that relax at a rate R . The statistical distribution of interaction strengths is characterized by a width Γ_{SD} . The weakly non-exponential 2-pulse echo shape shows that the bath relaxation rate occurs over timescales longer than T_{2e} , i.e. $Rt_{12} \ll 1$, so that the effective linewidth in Eq. 1 can be written as [24]

$$\Gamma_{eff}(t_{12}, t_{23}) = \Gamma_0 + \frac{1}{2}\Gamma_{SD}(Rt_{12} + 1 - e^{-Rt_{23}}). \quad (2)$$

To reduce the number of fit parameters, T_{1e} was directly determined from an exponential fit to the tail of the 3-pulse echo decays. Moreover, at the temperatures and low magnetic field used here, Γ_{SD} and the spin flip-flop rate R_{ff} are both temperature independent so that the relaxation rate R can be modeled as a function of the temperature T as $R = R_{ff} + \alpha_{O,g} \exp(-\Delta_g/T)$. The second term corresponds to a resonant two-phonon Orbach process where Δ is the energy of the lowest crystal field level above the ground state and α_O is the phonon

coupling coefficient. The two-phonon Raman and one-phonon direct terms are both negligible at the temperatures and magnetic field investigated. Γ_0 is also taken as independent of temperature. Fits of this model to the experimental 2- and 3- pulse echo decays (see Supplemental Material) give the following values: $\Gamma_0 = 2.7 \times 10^5$ Hz, $\Gamma_{SD} = 4.3 \times 10^5$ Hz, $R_{ff} = 2.1 \times 10^4 \text{ s}^{-1}$, $\alpha_{O,g} = 50 \times 10^{10}$ Hz and $\Delta_g = 40$ K.

The experimental parameters compare well with theoretical estimates for decoherence from spin flip flops of site 1 Er^{3+} ground-state spins (see Supplemental Material), with calculated values of $\Gamma_{SD,theory} = 4.4 \times 10^5$ Hz and $R_{ff,theory} = 1.6 \times 10^5 \text{ s}^{-1}$. The known splitting between the ground-state crystal field levels of 57 K [17] is larger than the fitted value, a known effect that is common in spin-lattice relaxation studies [25, 26]. For our magnetic field orientation, the ground-state effective g factor for site 1 and 2 spins is about 4 and 14 [22] so that the site 2 flip-flop rate is expected to be faster than for site 1 by a factor of roughly $(14/4)^4 = 150$. With this much faster rate, we expect decoherence caused by site 2 spins to be partially reduced due to the well-known "motional narrowing" effect [27]. Consequently, we attribute Γ_0 to site 2 ground-state spins that produce decoherence over sub- μ s timescales. This conclusion is supported by a simple theoretical estimate of $\Gamma_{0,theory} = 6 \times 10^5$ Hz for this effect that is consistent with the observed value (see Supplemental Material).

Fig. 3 shows the calculated variation of $T_{1g} = 1/R$ as a function of temperature. Below 2.2 K, relaxation is dominated by the flip-flop processes. A plot of T_{1e} extracted from Eq. 1 and the curve calculated from Eq. 2 by setting $t_{23} = 0$ is also displayed on Fig. 3B. The T_{1e} variations could be modeled by the sum of the optical excitation and emission rates combined with the Raman and Orbach spin relaxation processes (see Fig. 3B and Supplemental Material). At the lowest temperatures, T_1 reached 1.2 ms, limited by the optical stimulated emission rate $R_{opt} = 830$ Hz due to continuous excitation by the laser. In a pulsed configuration without laser excitation during the spin echo sequence, this would increase to the limit of $T_{1,opt} = 8$ ms [28].

For our experimental conditions, T_{2e} is limited by decoherence due to relaxation of ground-state spins. This decoherence could be considerably reduced by working at lower temperatures since the Orbach and Raman contributions quickly decrease as $\exp(-\Delta_e/T)$ and T^9 , respectively, while flip-flop rates decrease as $[\text{sech}(g_{eff}\mu_B B/2kT)]^2$, where k is the Boltzmann factor. For example, consider a weak field of 50 mT that is compatible with superconducting resonators and where the excited-state splitting is about 2 GHz, also in the range of typical microwave photons. At a temperature of 20 mK, decoherence only results from site 1 ground-state spin flip-flops because site 2 spins, with their large g factor, are completely polarized. The site 1 flip-flop rate

R_{ff} would be reduced by a factor $f = 2.9 \times 10^{-3}$ compared to 1.6 K, resulting in a spin coherence lifetime of $T_{2e} \approx 1/f\sqrt{\Gamma_{\text{SD}}R} = 2.9$ ms. This is likely to approach the decoherence limit due to ^{89}Y spins flips [24]. In contrast, even at very low temperatures, site 1 ground-state excitations will still experience rapid decoherence through the flip-flop process due to the large number of other resonant spins present in the lattice. In fact, spins excited into the higher energy spin state will have an increasing number of neighbors in the lower energy spin state that they can flip flop with as the temperature is decreased, resulting in an increase in the coherence decay rate up to twice the high-temperature rate. For our system, this effect will limit T_{2g} to less than 50 μs at the lowest temperatures. Moreover, a rephasing control pulse applied over the entire spin linewidth would cause a strong ISD effect, reducing T_{2g} to ~ 1 μs , independent of temperature (see Supplemental Material). These effects explain why we did not observe any ground state spin echo for the same conditions used for the excited state spin echo measurements. We also note that our analysis is also in qualitative agreement with the ground-state site 2 coherence lifetime of 5.6 μs that has been observed at 30 mK with a different magnetic field orientation [15].

Finally, we turn to an excited-state scheme for an optical to microwave transducer. Previous proposals used the ground-state spin transition by coupling it off-resonantly [10] or resonantly [11] to a microwave cavity. One of the limiting factors for efficient conversion in [11] is the short coherence lifetime compared to the coupling strength.

To take advantage of the potential increase in coherence time for the excited state, the protocol from [11] can be modified in the following way. The first step is the same as in [11], we start by preparing a narrow spectral feature and then apply a magnetic field gradient to broaden the feature. An incoming optical photon is then absorbed on the $|1\rangle - |4\rangle$ transition. The induced inhomogeneous broadening and the free evolution of the system lead to a dephasing of the optical coherence, preventing re-emission and ensuring that the optical photon is stored as a matter excitation. In the next step, we apply a π -pulse on the $|1\rangle - |3\rangle$ transition, bringing all of the population from state $|1\rangle$ to $|3\rangle$. The subsequent free evolution will further de-phase the system due to the inhomogeneous broadening of the spin state, but now at a possibly different rate. After a delay, we apply a second π -pulse to bring population back into $|1\rangle$, while simultaneously switching the field gradient to begin the rephasing procedure. Once the dephasing due to inhomogeneous broadening of the excited state is compensated, we apply another π -pulse, moving the population to the state $|3\rangle$ to complete the rephasing procedure, leaving the system in a collective state that strongly couples to a microwave cavity. Assuming the same spin-cavity coupling strength of $v/2\pi = 34$ MHz as in [15], which is justified since the principal values of the magnetic g tensors for

the $^4\text{I}_{15/2}$ and $^4\text{I}_{13/2}$ states in $\text{Er}^{3+}:\text{Y}_2\text{SiO}_5$ are roughly the same [22], and using our measured spin coherence lifetime for the excited state of $T_{2e} = 1.6$ μs (200 kHz homogeneous linewidth), we can estimate the conversion efficiency using Eq. 8 in [11] to be $\eta \gtrsim 99\%$. A further advantage of using the excited-state spin transition is the fact that only optically excited ions, i.e. those in the laser beam cross section, will interact with the microwave cavity, making spatial hole burning, which might be required in the previous proposals, superfluous. We note that the proposed protocol can also be reversed, i.e. it allows conversion of a microwave photon to a propagating telecom photon. Moreover, the bandwidth of the optical photon can be tuned in the protocol by controlling the strength of the field gradient.

In conclusion, we observed electron spin echoes in the optically excited state of an erbium doped crystal. Coherence lifetimes of up to 1.6 μs were recorded for a field of 8.7 mT at 1.9 K, and a detailed analysis of the decoherence processes suggest that ms lifetimes could be reached in conditions used in superconducting qubits studies. We propose a scheme to exploit these long coherence lifetimes for high efficiency, reversible optical to microwave conversion. Overall, the possibility of using excited-state spin transitions opens a new and attractive way to coherently interface RE ensembles with microwave cavities and may stimulate new proposals for transducer devices.

We thank M. Falamarzi, N. Sinclair, D. Oblak, and W. Tittel for useful discussions, and A. Marsh and R. Nerem for assistance during measurements. This work received funding from the French-US ANR project DIS-CRYS (No. 14-CE26-0037-01), US NSF grant no. CHE-1416454, Nano'K project RECTUS, the University of Calgary, and NSERC.

Note: A related experiment using nuclear hyperfine states in a $^{167}\text{Er}^{3+}$ -doped crystal has been performed in parallel.

-
- [1] C. W. Thiel, T. Böttger, and R. L. Cone, *J. Lumin.* **131**, 353 (2011).
 - [2] P. Goldner, A. Ferrier, and O. Guillot-Noël, *Handb. Phys. Chem. Rare Earths*, edited by J.-C. G. Bünzli and V. K. Pecharsky, Vol. 46 (Elsevier, Amsterdam, 2015) pp. 1–78.
 - [3] M. Zhong, M. P. Hedges, R. L. Ahlefeldt, J. G. Bartholomew, S. E. Beavan, S. M. Wittig, J. J. Longdell, and M. J. Sellars, *Nature* **517**, 177 (2015).
 - [4] C. Laplane, P. Jobez, J. Etesse, N. Gisin, and M. Afzelius, *Phys. Rev. Lett.* **118**, 210501 (2017).
 - [5] C. Clausen, I. Usmani, F. Bussieres, N. Sangouard, M. Afzelius, H. de Riedmatten, and N. Gisin, *Nature* **469**, 508 (2011).
 - [6] F. Bussieres, C. Clausen, A. Tiranov, B. Korzh, V. B. Verma, S. W. Nam, F. Marsili, A. Ferrier, P. Goldner, H. Herrmann, C. Silberhorn, W. Sohler, M. Afzelius, and

- N. Gisin, *Nat. Photonics* **8**, 775 (2014).
- [7] N. Maring, P. Farrera, K. Kutluer, M. Mazzera, G. Heinze, and H. de Riedmatten, *Nature* **551**, 485 (2017).
- [8] J. G. Bartholomew, K. de Oliveira Lima, A. Ferrier, and P. Goldner, *Nano Lett.* **17**, 778 (2017).
- [9] T. Zhong, J. M. Kindem, J. G. Bartholomew, J. Rochman, I. Craiciu, E. Miyazono, M. Bettinelli, E. Cavalli, V. B. Verma, S. W. Nam, F. Marsili, M. D. Shaw, A. D. Beyer, and A. Faraon, *Science (80-.)*. **357**, 1392 (2017).
- [10] L. A. Williamson, Y. H. Chen, and J. J. Longdell, *Phys. Rev. Lett.* **113**, 203601 (2014).
- [11] C. O'Brien, N. Lauk, S. Blum, G. Morigi, and M. Fleischhauer, *Phys. Rev. Lett.* **113**, 063603 (2014).
- [12] X. Fernandez-Gonzalvo, Y. H. Chen, C. Yin, S. Rogge, and J. J. Longdell, *Phys. Rev. A* **92**, 062313 (2015).
- [13] Y. H. Chen, X. Fernandez-Gonzalvo, and J. J. Longdell, *Phys. Rev. B* **94**, 075117 (2016).
- [14] S. Probst, H. Rotzinger, A. V. Ustinov, and P. A. Bushev, *Phys. Rev. B* **92**, 014421 (2015).
- [15] S. Probst, H. Rotzinger, S. Wünsch, P. Jung, M. Jerger, M. Siegel, a. V. Ustinov, and P. a. Bushev, *Phys. Rev. Lett.* **110**, 157001 (2013).
- [16] E. Z. Cruzeiro, A. Tiranov, J. Lavoie, A. Ferrier, P. Goldner, N. Gisin, and M. Afzelius, *ArXiv* , 1 (2017), arXiv:1712.02682.
- [17] T. Böttger, Y. Sun, C. W. Thiel, and R. L. Cone, *Phys. Rev. B* **74**, 075107 (2006).
- [18] E. Saglamyurek, T. Lutz, L. Veissier, M. P. Hedges, C. W. Thiel, R. L. Cone, and W. Tittel, *Nat. Photonics* **9**, 83 (2015).
- [19] J. Mlynek, N. C. Wong, R. G. DeVoe, E. S. Kintzer, and R. G. Brewer, *Phys. Rev. Lett.* **50**, 993 (1983).
- [20] C. Li, C. Wyon, and R. Moncorge, *IEEE J. Quantum Electron.* **28**, 1209 (1992).
- [21] O. Guillot-Noël, P. Goldner, Y. Du, E. Baldit, P. Monnier, and K. Bencheikh, *Phys. Rev. B* **74**, 214409 (2006).
- [22] Y. Sun, T. Böttger, C. W. Thiel, and R. L. Cone, *Phys. Rev. B* **77**, 085124 (2008).
- [23] W. Mims, *Phys. Rev.* **168**, 370 (1968).
- [24] T. Böttger, C. W. Thiel, Y. Sun, and R. L. Cone, *Phys. Rev. B* **73**, 075101 (2006).
- [25] B. A. Young and H. J. Stapleton, *Phys. Lett.* **21**, 498 (1966).
- [26] G. Wolfowicz, H. Maier-Flaig, R. Marino, A. Ferrier, H. Vezin, J. J. L. Morton, and P. Goldner, *Phys. Rev. Lett.* **114**, 170503 (2015).
- [27] N. Bloembergen, E. M. Purcell, and R. V. Pound, *Phys. Rev.* **73**, 679 (1948).
- [28] C. W. Thiel, W. R. Babbitt, and R. L. Cone, *Phys. Rev. B - Condens. Matter Mater. Phys.* **85**, 1 (2012).